Mechanics of Advanced Composite Structures 6 (2019) 167 – 179

Semnan University

Mechanics of Advanced Composite Structures

journal homepage: http://MACS.journals.semnan.ac.ir

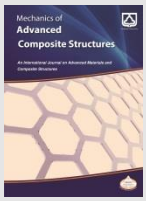

Thermoelastic Analysis of Compressor Spool in Turbojet Engine and Redesign it Using Functionally Graded Materials with Optimal Coefficients

B. Shahriari [a*], M.S. Sadeghinezhad [b], S. Yousefi [a]

[a] *Department of Mechanical Engineering, Malek Ashtar University of Technology, Isfahan, Iran*
[b] *Department of Engineering, University of Isfahan, Isfahan, Iran*

PAPER INFO

Paper history:
Received 2018-05-02
Received in revised form 2019-01-15
Accepted 2019-04-26

Keywords:
Turbojet Engine
Compressor Spool
Thermoelastic Analysis
Functionally Graded Material

ABSTRACT

In this article, an exact analysis of compressors spool in a turbojet engine has been investigated. The spool is modeled as a rotating thick-walled hollow circular cylinder with free-clamp ends. It is subjected to centrifugal load due to its constant rotational speed, uniform internal and external radial loads and arbitrary thermal gradients. The analysis is initially investigated for the homogeneous state. Then FGM state is investigated to improve the safety factor of the spool. In order to calculate the safety factor, Von-Mises criterion has been used. In FGM state, thermoelastic properties of material would vary in radial direction. The function of these properties changes is assumed exponential. To obtain the highest safety factor, the numerical optimization method has been used and the optimal results have been compared with the homogeneous state. To drive the relations for free-clamp ends boundary condition, at first spool is considered clamp-clamp ends. Then, the effect of releasing one of the ends has been calculated and finally, using the principle of superposition, the results for clamp-free ends state has been investigated. In addition, the effect of changing the non-homogeneous coefficients, spool rotating speed, radial loads and thickness on the safety factor are investigated. Increasing the thickness and radial loads would lead to a change in the optimal coefficient and would result in reducing the safety factor of optimum state. The results showed that utilization of FGM state with optimal coefficient could significantly increase the safety factor and reduce displacements. Furthermore, increasing the rotation speed and radial loads would result in a change in the optimal non-homogeneous coefficient and reduce its equivalent safety factor.

© 2019 Published by Semnan University Press. All rights reserved.

1. Introduction

In recent years, with the increasing growth of various industries and the development of advanced industrial compressors, axial compressors have been widely used in many industries such as aerospace, turbines, reactors and other rotary machines. One of the rotating parts in this type of compressors is a spool, which is very important due to the thermo-mechanical loads applied on it. The spool is a rotary structure that in recent years has been widely used in various sectors such as aerospace industries and nuclear facilities and has a very similar geometry to a thick-walled circular cylinder. This structure is under thermo-mechanical loads. Analysis of compressors rotating spool stresses and obtaining reliable safety factor is very important in the design of a turbojet compressor. One of the methods for increasing the safety factor is changing the basic material of structures. A bunch of useful materials are FGM materials with a non-homogeneous coefficient which is suitable for redesigning a spool with a higher safety factor. FGM

* Corresponding author. Tel.: +98-9131254280; Fax: +98-31-45227136
E-mail address: shahriari@mut-es.ac.ir

DOI: 10.22075/macs.2019.14686.1144

materials are special types of composites and their properties can change steady and slowly in one or more arbitrary directions. These materials have high mechanical strength at high temperatures against applied loads, that makes them an appropriate selection in the above activity. Analytical solution for rotating thick-walled hollow circular cylinder problems has been investigated in most standard elasticity books such as Nadai [1], Timoshenko and Goodier [2] using the plane strain assumption. Using Kirchhoff-Love hypothesis, Lamé [3] presented an analytical solution for thick-walled cylinders under both inner and outer pressures. Fukui and Yamanaka [4] studied the elastic problem of thick-walled tubes of an FGM under internal pressure assuming the plane strain. Using the infinitesimal theory of elasticity, Tutuncu and Ozturk [5] presented an exact solution for obtaining stresses and displacements in FG cylindrical and spherical vessels subjected to internal pressure. Rooney and Ferrari [6] investigated an analytical solution for FGM cylinders under tension and bending and concluded that by changing the modulus of elasticity, they could improve the cylinder behavior in tension and bending. Galic and Horgan [7] developed an analytic solution to axisymmetric problem of an infinitely long, radially polarized, radially orthotropic piezoelectric hollow circular cylinder rotating about its axis at a constant angular velocity. Tutuncu [8] obtained a tractable solution rather than numerical results to allow for further parametric studies. Stress and displacement solutions in the form of power series are presented in FGM thick-walled cylinders with exponentially-varying elastic modulus in the radial direction. Khoshgoftar et al. [9] presented an analytical solution for FG thick cylinders with Finite length under longitudinally non-uniform pressure. Zamani Nejad et al. [10] provided a semi-analytic solution for determining the stresses and displacements in rotating cylindrical shells with a variable thickness under uniform pressure. Ghajar et al. [11] investigated the thermo-visco-elastic response for symmetric FGM rotating thick cylindrical pressure vessels under arbitrary boundary and initial conditions using finite element methods. Nejad et al. [12] investigated an elastoplastic analysis of rotating thick-walled cylindrical pressure vessels made of FGMs. The stresses in plastic fields and displacements were obtained using the Tresca criterion. Arefi et al. [13] investigated the thermo-elastic analysis of a rotating hollow cylinder made of arbitrary FGMs. System responses were obtained for temperature distribution, radial displacement and radial and circumferential stresses in general state. Jabbari et al. [14] presented a comparative study of thermoelastic analysis given for material properties and disk thickness profiles using the Lamé problem subjected to body force, internal and thermal loads. Anani and Rahimi [15] investigated a rotating cylindrical shell made of functionally graded incompressible hyperelastic materials using hyperelastic theory. This analysis was based on two main assumptions; material was incompressible and material properties vary only in radial direction of the cylinder. Afshin et al. [16] studied the transient thermoelastic analysis of FGM rotating thick cylindrical pressure vessels under arbitrary boundary and initial conditions using an exact solution and compared it with numerical results from previous studies. Gharibi et al. [17] performed an elastic analysis of FG rotating thick cylindrical pressure vessels with exponentially-varying properties using power series method of Frobenius. They finally compared the effects of the changes in some of the parameters, such as rotation speed in their results. Jalali and Shahriari [18] presented an elastic stress analysis of rotating variable thickness annular disk made of FGM using finite difference method. They investigated the effects of various geometric and material properties on the stresses and radial deflection. Khorsand et al. [19] presented a method to see the weight optimization for FG rotating disks with variable thickness under thermoelastic loading. In this analysis, they used a combination of a coevolutionary particle swarm optimization (CPSO) approach coupled with a differential quadrature (DQ) method applied to obtain the minimized stress and displacement fields through the geometry of the disk. Hosseini et al. [20] studied the strain effects on the thermoelastic analysis of a functionally graded micro-rotating cylinder using GDQM. NKene et al. [21] evaluated the displacements, strains, and stresses of in an inhomogeneous rotating hollow cylinder made of functionally graded materials under axisymmetric radial loadings using the shooting method and the fourth order Runge-Kutta algorithm. Parhizkar et al. [22] studied the stress and active control analysis of functionally graded piezoelectric material cylinder and disk under electro-thermo-mechanical loading. Mehditabar et al. [23] analyzed a functionally graded piezoelectric rotating hollow cylindrical shell subjected to thermo-elastic dynamic loads. Hussain et al. [24] studied the thermo elasto-plastic analysis of rotating axisymmetrical bodies in terms of modified von-Mises yield criterion.

In this article, analyzing and redesigning a spool with a coefficient for properties function in an axial compressor has been studied. In order to investigate

the spool according to its structure, a thermoelastic analytical solution is performed for a rotating spool in an axial compressor made of FGMs under internal and external loading with free-clamp ends. The material properties are assumed to vary nonlinearly in the radial direction and the Poisson's ratio is assumed constant. At first, differential equation of motion for FGM material is derived by assuming the properties functions exponentially and thermal gradients as an arbitrary function of radius. Then the equation is solved analytically using MATLAB. Stresses and displacements were initially calculated in clamp-clamp ends boundary conditions. Then, separately, the effect of the releasing one of the ends was investigated and the spool stresses and displacements in free-clamp ends condition were calculated using the principle of superposition. Then, the governing thermal differential equation of the spool was solved and the response was replaced with arbitrary thermal function considered at first stage of the analysis. After calculating the displacements and stresses applied to spool, using the numerical optimization method, the non-homogeneous coefficient, which leads to the highest safety factors, was calculated. In addition, changes in the values of different parameters affecting the stresses and displacements, including rotation speed, magnitude, and type of loading on external surface in the same working conditions on optimal non- homogeneous coefficient have been investigated.

2. Mathematical Formulation

Fig. 1 shows a front view of a spool in an axial compressor. The spool has an inner and outer radius and is under internal and external uniform radial loading represented by, r_i, r_o, P_i and P_o respectively. In addition, the spool is rotating with constant angular velocity around its axial direction. However, due to the axial symmetry in the properties distribution and geometry, it was assumed that the radial displacement is only a function of the radius (u=u(r)) and the circumferential displacement and shear stress would be ignored.

By applying equilibrium relations in radial direction, the governing equilibrium equation of motion in the spool was obtained as:

$$\frac{d\sigma_r}{dr}+\frac{\sigma_r-\sigma_\theta}{r}+\rho r\omega^2=0 \tag{1}$$

in which, σ_r and σ_θ are the radial and circumferential stresses respectively; also, ρ and ω respectively correspond to the density and rotation speed of the spool. In Eq. (2), the compatibility equations, representing the relations between strain and displacements, are shown after applying the plane strain assumption:

$$\varepsilon_r=\frac{du}{dr}\quad \&\quad \varepsilon_\theta=\frac{u}{r}\quad \&\quad \varepsilon_z=\frac{dw}{dr}=0 \tag{2}$$

where ε_r, ε_θ and ε_z are normal strains in radial, circumferential and axial directions, respectively. Furthermore, u, v and w are displacements in radial, circumferential and axial directions, respectively.

Using the plane elasticity theory for infinitesimal displacements under plane strain assumptions, the constitutive equations representing the thermoelastic relations between strains and stresses are written simpler for homogeneous and isotropic materials, known as Hooke's relationships as follow:

$$\begin{aligned}\sigma_r&=\frac{E}{1+\nu}\left[\frac{\nu}{1-2\nu}(\varepsilon_r+\varepsilon_\theta+\varepsilon_z)+\varepsilon_r\right]\\&-\frac{E}{1-2\nu}\alpha T(r)\\\sigma_\theta&=\frac{E}{1+\nu}\left[\frac{\nu}{1-2\nu}\varepsilon_r+\varepsilon_\theta+\varepsilon_z+\varepsilon_t\right]\\&-\frac{E}{1-2\nu}\alpha T(r)\\\sigma_z&=\frac{E}{1+\nu}\left[\frac{\nu}{1-2\nu}\varepsilon_r+\varepsilon_\theta+\varepsilon_z+\varepsilon_z\right]\\&-\frac{E}{1-2\nu}\alpha T(r)\end{aligned} \tag{3}$$

where ν is Poisson's ratio, E is the modulus of modulus of elasticity, α is the thermal expansion coefficient, and T(r) is heat distribution function, which is assumed to be arbitrary and a function of radius.

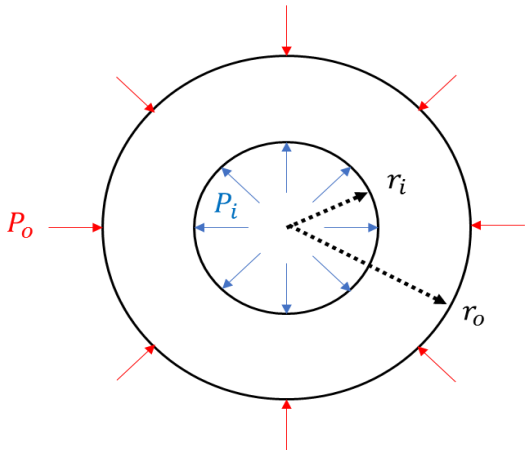

Fig. 1. Axial Compressor spool front view

By substituting Eq. (2) into Eq. (3), the relations representing the stresses in terms of displacement as the following expression could be obtained:

$$\sigma_r = \frac{E}{(1+\nu)(1-2\nu)} \times \left[(1-\nu)\frac{du}{dr} + \nu\frac{u}{r} - (1+\nu)E\alpha T(r)\right]$$

$$\sigma_\theta = \frac{E}{(1+\nu)(1-2\nu)} \times \left[\nu\frac{du}{dr} + (1-\nu)\frac{u}{r} - (1+\nu)E\alpha T(r)\right] \quad (4)$$

$$\sigma_z = \frac{E\nu}{(1+\nu)(1-2\nu)}\left[\frac{du}{dr} + \frac{u}{r}\right] - \frac{E}{1-2\nu}\alpha T(r)$$

In the following, considering the spool properties function in FGM state, including the modulus of elasticity, density, thermal expansion coefficient, thermal conductivity and yield strength, which is considered as an exponential function and variable in radial direction as follows:

$$\begin{aligned} E(r) &= E_i\left(\frac{r}{r_i}\right)^m \\ \rho(r) &= \rho_i\left(\frac{r}{r_i}\right)^m \\ \alpha(r) &= \alpha_i\left(\frac{r}{r_i}\right)^m \\ k(r) &= k_i\left(\frac{r}{r_i}\right)^m \\ \sigma_y(r) &= \sigma_{y_i}\left(\frac{r}{r_i}\right)^m \end{aligned} \quad (5)$$

where, E_i, ρ_i, α_i, k_i and σ_{y_i} respectively, are the modulus of elasticity, density, thermal expansion coefficient, thermal conductivity, and the yield strength at inner radius, m is the non-homogeneous coefficient and is considered to have a constant value. Also, r_i is the inner radius of the spool. By substituting Eq. (5) into Eq. (4), the relationship between stresses and radial displacement for the FGM spool with the exponential properties function would be obtained as follows:

$$\begin{aligned} \sigma_r &= \frac{E_i\left(\frac{r}{r_i}\right)^m}{(2\nu-1)(\nu+1)}\left[(\nu-1)\frac{du}{dr} - \frac{\nu u(r)}{r}\right] \\ &+ \frac{\alpha_i E_i\left(\frac{r}{r_i}\right)^{2m} T(r)}{2\nu-1} \\ \sigma_\theta &= \frac{E_i\left(\frac{r}{r_i}\right)^m}{(2\nu-1)(\nu+1)} \times \left[(-\nu)\frac{du}{dr} + \frac{(1-\nu)u(r)}{r}\right] \\ &+ \frac{\alpha_i E_i\left(\frac{r}{r_i}\right)^{2m} T(r)}{2\nu-1} \\ \sigma_z &= \frac{\nu E_i\left(\frac{r}{r_i}\right)^m}{(2\nu-1)(\nu+1)}\left[\frac{du}{dr} + \frac{u(r)}{r}\right] \\ &+ \frac{2\nu\alpha_i E_i\left(\frac{r}{r_i}\right)^{2m} T(r)}{2\nu-1} \end{aligned} \quad (6)$$

Substituting Eq. (6) into Eq. (1), the differential equation of the motion in FGM spool is obtained as follows:

$$\begin{aligned} &r^2\frac{d^2u}{dr^2} + r(1+m)\frac{du}{dr} \\ &- \frac{\left(1-\nu(m+1)\right)}{1-\nu}u(r) \\ &+ \frac{\rho_i r^3\omega^2(\nu+1)(1-2\nu)}{E_i(1-\nu)} - \frac{(\nu+1)\alpha_i}{(1-\nu)r_i^m} \times \\ &\left\{\frac{r^{m+2}dT(r)}{dr} + 2mr^{m+1}T(r)\right\} = 0 \end{aligned} \quad (7)$$

By solving the differential Eq. (7) exactly by using mupad parametric coding in MATLAB, radial displacement could be obtained as follows:

$$\begin{aligned} u(r) &= C_1A_3 - \frac{C_2A_3}{r^H H} \\ &+ \frac{A_3}{H}\int_{r_i}^{r} r^{\frac{m}{2}}\frac{(\nu+1)A_1}{r^{\frac{H}{2}}(A_2)}dr \\ &- \frac{A_3}{r^H H}\int_{r_i}^{r} r^{\frac{H+m}{2}}\frac{(\nu+1)A_1}{A_2}dr \end{aligned} \quad (8)$$

where A_1, A_2 and A_3 are:

$$\begin{aligned} A_1 &= (2\nu-1)\rho_i r^2\omega^2\left(\frac{r}{r_i}\right)^m \\ &+ E_i\alpha_i\left(\frac{r}{r_i}\right)^{2m}\left[\frac{rdT(r)}{dr} + 2m\big(T(r)\big)\right] \\ A_2 &= E_i\left(\frac{r}{r_i}\right)^m(1-\nu) \\ A_3 &= r^{\frac{H-m}{2}} \end{aligned} \quad (9)$$

In addition, in Eq. (8) and Eq. (9), H is a constant value and is:

$$H = \sqrt{\frac{4\nu + 4m\nu + m^2\nu - m^2 - 4}{\nu - 1}} \quad (10)$$

In Eq. (8), C_1 and C_2 are integration constants and will be determined according to the boundary conditions. By substituting Eq. (8) into Eq. (6), the

radial, circumferential and axial stresses are obtained as follows:

$$\sigma_r = (B_2B_3)\times \left\{\left(\frac{B_1}{r}\right)(B_4+C_1) - \frac{(B_5+C_2)(H+B_1)}{Hr^{H+1}}\right\} - \left(\frac{\nu B_2B_3}{r(1-\nu)}\right)\left\{\frac{[Hr^H(B_4+C_1)-(B_5+C_2)]}{Hr^H}\right\}$$

$$\sigma_\theta = \left(\frac{\nu B_2B_3}{(1-\nu)}\right)\times \left\{\frac{(B_5+C_2)(H+B_1)}{Hr^{H+1}} - \left(\frac{B_1}{r}\right)(B_4+C_1)\right\} + \left(\frac{B_2B_3}{r}\right)\left\{\frac{[Hr^H(B_4+C_1)-(B_5+C_2)]}{Hr^H}\right\} \quad (11)$$

$$\sigma_z = \left(\frac{\nu B_2B_3}{1-\nu}\right)\left[-HB_1r^{H-1}(B_4+C_1) + \frac{(B_5+C_2)(H+B_1)}{Hr^{H+1}} + \frac{[Hr^H(B_4+C_1)-(B_5+C_2)]}{Hr^H}\right]$$

where the B_i parameters are:

$$B_1 = \frac{m-H}{2} \quad (12)$$

$$B_2 = r^{B_1}$$

$$B_3 = \frac{E_i(1-\nu)\left(\frac{r}{r_i}\right)^m}{(2\nu-1)(\nu+1)}$$

$$B_4 = \int_{r_i}^{r} \frac{A_1(1+\nu)r^{\frac{m}{2}}}{HB_3\sqrt{r^H}}dr$$

$$B_5 = \int_{r_i}^{r_o} \frac{A_1(1+\nu)r^{\frac{m+H}{2}}}{B_3}dr$$

where r_o is the spool outer radius. To determine the C_1 and C_2 constants, considering that the spool is under uniform internal P_i and external loads P_o at the inner and outer radius, respectively. Therefore, the boundary conditions are as follows:

$$@\ r = r_i \rightarrow \sigma_r = P_i$$
$$@\ r = r_o \rightarrow \sigma_r = P_o \quad (13)$$

Substituting Eq. (13) into Eq. (11) gives a linear system of equation consists of missing constants (C_1 and C_2). By solving the equations system, the integral constants are determined as follows:

$$C_1 = \frac{2(2\nu-1)(\nu+1)}{E_iD_2D_5}\times \left[D_3r_i^{\frac{H+m+2}{2}} - \frac{D_1r_o^{\frac{H+m+2}{2}}}{\left(\frac{r}{r_i}\right)^{m1}}\right] \quad (14)$$

$$C_2 = \frac{2H(2\nu-1)(\nu+1)}{E_iD_2D_4}\times \left[D_3{r_o}^Hr_i^{\frac{H+m+2}{2}} - \frac{D_1r_i^Hr_o^{\frac{H+m+2}{2}}}{\left(\frac{r}{r_i}\right)^m}\right] \quad (15)$$

where D_i, B_i and A_i can be extracted in Eqs. (16), (12) and (9), respectively.

$$D_1 = +\frac{\left(\frac{r}{r_i}\right)^m E_i}{(2\nu-1)(\nu+1)}\left\{r_o^{\frac{H-m-2}{2}}D_8\left[\binom{\nu}{+(\nu-1)}\left(\frac{m-H}{2}\right)\right] - \frac{D_9\big(2\nu+(m+H)(\nu-1)\big)}{2Hr_o^{\frac{H+m+2}{2}}}\right\} + P_o - \frac{\alpha_i\left(\frac{r}{r_i}\right)^{2m}E_iT(r_o)}{(2\nu-1)}$$

$$D_2 = r_o^H - r_i^H$$

$$D_3 = \frac{P_i - \alpha_iE_iT(r_i)}{(2\nu-1)} \quad (16)$$

$$D_4 = 2\nu + (m1+H)(\nu-1)$$

$$D_5 = 2\nu + (m1-H)(\nu-1)$$

$$D_6 = E_i(1-\nu)\left(\frac{r}{r_i}\right)^m$$

$$D_7 = r^{\frac{H}{2}}D_6H$$

$$D_8 = \int_{r_i}^{r_o}\frac{A_1(1+\nu)r^{\frac{m}{2}}}{D_7}dr$$

$$D_9 = \int_{r_i}^{r_o}\frac{A_1(1+\nu)r^{\frac{m+H}{2}}}{D_6}dr$$

By substituting the calculated C_1 and C_2 into Eq. (8) and (11), radial displacement and stresses in clamp-clamp condition could be obtained, respectively. In addition, von Mises criterion was used to calculate the equivalent stress.

It is obvious that by setting the non-homogeneous constant (m) zero in Eqs. (8) and (11), respectively, radial displacement and stresses can be calculated for a homogeneous state.

In free-clamp ends boundary condition, given that there is no external axial force to satisfy the axial stress σ_z in Eq. (11), and on the other hand, according to the stress distribution shown in Fig. 2 which is set for free-clamp ends condition, Eq. (11) is not able to show the real axial stress for the spool. Therefore, in order to satisfy the equilibrium equation in axial direction, the effective axial stress

which represented by σ'_z should have the axial force in each section and must be perpendicular to the axial direction and in a distance far enough from clamp end should be zero. Therefore, the pure axial load across the entire cross section must be zero. For the surface element shown in Fig. 2, the following equation must be established [25].

$$F'_z = \int \sigma'_z dA = 2\pi \int \sigma'_z r dr \tag{17}$$

where F'_z, σ'_z and dA are axial loading, axial stress with free ends and elements cross-section area, respectively.

To satisfy this equilibrium condition in axial direction, a new system of stresses $\overline{\sigma_r}$, $\overline{\sigma_\theta}$, and $\bar{\sigma}_z$ must be superposed to the system of stresses σ_r, σ_θ, and σ_z which were calculated earlier. This new system of stresses fulfilling all conditions must be the following:

$$\overline{\sigma_\theta} = \overline{\sigma_r} = 0 \tag{18}$$
$$\bar{\sigma}_z = \text{Constant}$$

It is obvious that the radial and circumferential stresses would not change with the superposition of these two stress systems, while the effective axial stress σ'_z will be given by the sum of stress σ_z, which is distributed on the generic cross-section according to a nonlinear function of the radius and satisfies the plane strain state assumption ($\varepsilon_z = 0$), and of stress $\bar{\sigma}_z$, which is distributed uniformly on the same section, so that the latter can remain plane and perpendicular to the axis in compliance with the assumption (2) of a strain state characterized by a uniform axial translation of a generic cross section. In this case, assumption which makes it possible to write the following relation is as follows:

$$\varepsilon'_z = \varepsilon_z + \bar{\varepsilon}_z = \bar{\varepsilon}_z = \text{Constant} \tag{19}$$

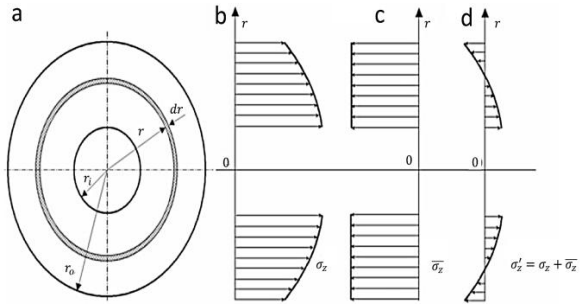

Fig. 2. Axial stresses in a rotating spool: (a) element area of the cross section away from the ends; (b) axial stress σ_z with clamped ends (c) uniform stress $\bar{\sigma}_z$ (d) axial stress σ'_z with free ends [25]

To determine σ'_z Eq. (17) could be utilized by setting the relation below:

$$\sigma'_z = \sigma_z + \bar{\sigma}_z \tag{20}$$

Moreover, by substituting Eq. (20) into Eq. (17):

$$\int_{r_i}^{r_o} (\sigma_z + \bar{\sigma}_z) r dr = 0 \tag{21}$$

By integrating the Eq. (21), $\bar{\sigma}_z$ is calculated. Then substituting $\bar{\sigma}_z$ (Eq. (21)) and σ_z (Eq. (11)) into Eq. (20), the effective axial stress of the spool in free-clamp ends condition can be calculated. Also, by substituting Eq. (2) which results in $w = z\varepsilon_z$, into Hooke's relationships (Eq. (3)) and Eq. (10), axial and radial displacements can be calculated, respectively.

3. Thermal Equation

According to the small differences between the spool temperature at the ends (free end against clamped end), the thermal distribution can be assumed as one-dimensional heat conduction. In the steady state case, the heat conduction equation for the one-dimensional problem in cylindrical coordinates would be simplified to [26]:

$$\frac{\partial}{\partial r}\left(kr\frac{\partial T}{\partial r}\right) = 0 \tag{22}$$

To solve the thermal differential equation, the thermal boundary conditions for an FGM hollow cylinder is given as:

$$@\, r = r_i \rightarrow k\frac{dT}{dr} = h_i(T - T_i) \tag{23}$$
$$@\, r = r_o \rightarrow -k\frac{dT}{dr} = h_o(T - T_o)$$

where T_i and T_o are the temperatures of the surrounding media, h_i and h_o are the heat transfer coefficients and subscripts i and o correspond to inner and outer surfaces, respectively. The general solution of Eq. (22) considering the thermal transfer coefficient for FGM state (Eq. (5)), and boundary conditions (Eq. (23)) is:

$$T(r) = \frac{T_1 r + T_2}{T_3} \tag{24}$$

where β is dimensionless radial coordinate and considered as follows:

$$\beta = \frac{r_i}{r_o} \tag{25}$$

$$T_1 = \frac{(T_i - T_o)}{mr_i}$$

$$T_2 = \frac{k_i(T_i + T_o)}{r_i h_i} + k_i T_i \left(\frac{1}{r_o h_o} - \frac{1}{r_i h_i}\right)$$

$$T_3 = k_i \left(\frac{1}{r_i h_i} + \frac{1}{r_o h_o}\right) + \frac{(1-\beta^m)}{m}$$

4. Safety Factor Optimization

It is obvious that considering any arbitrary non-homogeneous coefficient (m), will result in unique stresses and displacement distribution in the spool analysis. So, in order to find a specific coefficient which leads to the highest safety factor, using an optimization method is recommended. One of the optimization methods widely used for functions with limited domain range is numerical method. In this method, initially due to the limited function range, instead of analysis for all continuous points which are infinitive in domain range, there is a need to analyze n times for n discrete points selected in positions with same distance in domain range and the point leading to best safety factor has been introduced as an optimized non-homogeneous coefficient. Obviously, using more discrete points with less distance would lead to answers much closer to reality. In this method, increasing the discrete points will be continued until convergence of the solution occurs. Hence, obtained stresses and displacement distribution in FGM state is coded in MATLAB and the optimized m constant leading to highest safety factor would be found.

Note that yield strengths for homogeneous materials are constant and for FGM materials would be calculated according to Eq. (5).

5. Spool Analysis

To analyze the spool in axial compressor, it is modeled as a rotating thick-walled cylinder with free-clamp ends. Analytical solution for determining the stresses, displacements, and strains for both homogeneous and FGM states were explained in Section 2. In order to analyze the existing spool, geometric and thermo-mechanical characteristics were considered as follow: internal and external radius of the spool are 40cm and 48cm, respectively; the spool length is 40cm and has a uniform rotational speed of 16200 rpm. The temperature at the inner and outer surfaces of the spool are 4 °C and 50°C, respectively. The spool is also selected as Ti6Al4V-Annealed (Grade V). In this way, the modulus of elasticity is 119 GPa, density is 7860 Kg/m^3, Poisson's ratio is 0.31. The thermal expansion coefficient is $6(10^{-9})\,1/℃$, and the yield strength is 1100 MPa. It was also assumed that there is no heat transfer taking place between the inner and outer surfaces with the surrounding medium (h_i & $h_o \rightarrow \infty$). After calculating the results for homogeneous state, the numerical method was used to find the optimal non-homogeneous coefficient leading to highest spool safety factor. The non-homogeneous FGM coefficient is an arbitrary value considered in limited and different domain ranges according to previous studies [15], [27] and [28], the range is always between -10 to 10. Here, to ensure that a more complete range is investigated, the wider range from -50 to 50 has been considered. According to numerical method, the distance between the solving points has started from 1. By reducing distance at each step, in points with distance of 1/10000, the convergent optimal coefficient has been calculated. Fig. 3, shows changing the spool minimum safety factor for the selected non-homogeneous coefficient in a finite range of -50 to 50 for points with distance of 1/10000. Obviously, the positive coefficients are not suitable for considered spool at all, and choosing positive coefficients leads to safety factors less than one, resulting in failure of the spool. The highest safety factor will appear in the negative region and with the value of -8.975. For this coefficient (optimal FGM state), the calculated safety factor is 5.058, which shows a 477.16% improvement in comparison with the safety factor in homogeneous state (1.06). It is also clear that with the departure of the selected coefficient from optimal coefficient (-8.975), safety factor will be reduced greatly, reaching the coefficients -20 and +0.4 will put the spool at its critical level ($S_f \cong 1$). Therefore, due to the constraints and limitation on FGM fabrication, the FGM material with a non-homogeneous coefficient was selected which is closest to the theoretical calculated optimal coefficient (-8.975).

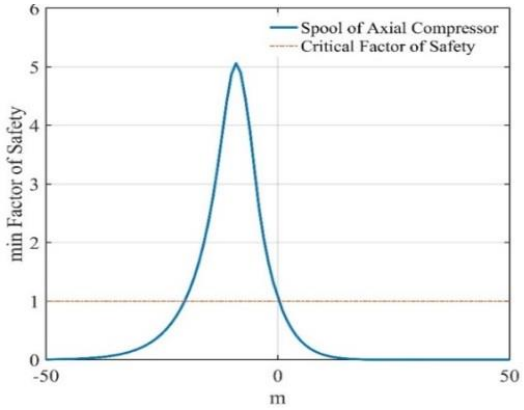

Fig. 3. Determining the optimal FGM Spool using the numerical optimization method with the discrete points distance of 1/10000

Fig. 4 presents the distribution of optimal FGM properties. It could be seen that all properties are decreasing along radius.

Fig. 5 presents the distribution of radial stresses of spool in homogeneous and optimum FGM states. In addition, Fig. 6 presentsthe distribution of circumferential stresses of the spool in homogeneous and optimum FGM states. It is clear that the inner surface of the spool is under higher stresses in comparison with outer surface, and the maximum value of circumferential stress in optimal state has decreased extremely (over ten times) in comparison with homogeneous state. Fig. 7 indicates the distribution of axial stresses of the spool in homogeneous and optimum FGM states. It could be seen that behavior of stress distribution in optimal state has changed in comparison with homogeneous state. In homogeneous state, axial stresses are mainly in tensile region, while in optimal state, they are mainly in pressure region**.** Axial stress behavior is ascending in optimal state, stresses are located in pressure region and along with increasing radius, the stress value forwarding to zero and this shows that optimal axial stresses decreased in comparison with homogeneous state.

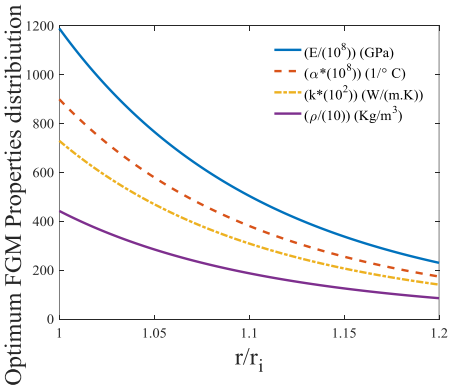

Fig. 4. Determining the optimal FGM Spool using the numerical optimization method with the discrete points distance of 1/10000

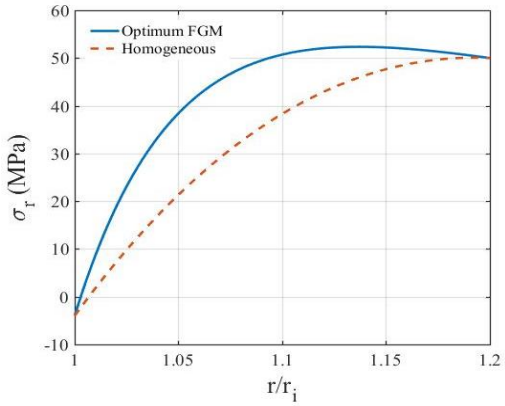

Fig. 5. Distribution of radial stresses in homogeneous and optimal FGM states

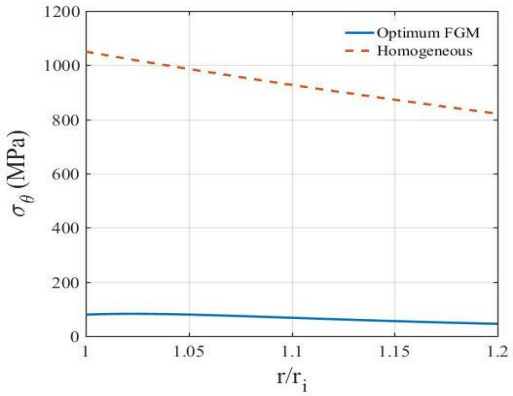

Fig. 6. Distribution of circumferential stresses in homogeneous and optimal FGM states

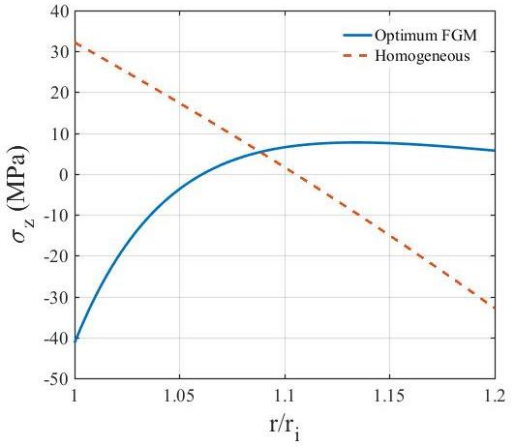

Fig. 7. Distribution of axial stresses in homogeneous and optimal FGM states

Fig. 8 shows the distribution of von Mises stresses of spool in homogeneous and optimum FGM states. After changing the spool homogeneous material into optimal FGM more than 5 times reduction in maximum value of von Mises equivalent stress is expected. Furthermore, in the spool, the stresses at internal surface are higher than those of outer surface. The difference between stress values range in both surfaces is higher in homogeneous state.

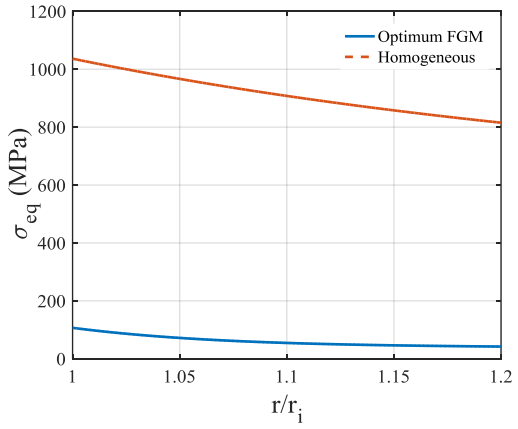

Fig. 8. Distribution of Von Mises equivalent stress in homogeneous and optimal FGM states

Fig. 9 presents the distribution of radial displacement in homogeneous and optimal FGM states. It is clear that using an optimum FGM will result in a reduction of about 89.68% within the range of radial displacement. In addition, Fig. 10 presents the distribution of axial displacement in homogeneous and optimal FGM states. In both cases, the maximum axial displacement has negative values and occurs in free side and it is obvious that axial displacement is zero in clamped side of the spool. In the optimum state, the axial displacement is reduced by 54.6% in comparison with homogeneous state.

Also, Figs. 11 to 13 present the distribution of radial, circumferential, and axial normal strains of the spool in homogeneous optimal FGM states. In all the cases, the results indicate that the optimal strain values reduced in comparison with homogeneous strain. In radial, circumferential and axial strains, the maximum values of strains result for optimal state have decreased by 37.35, 44.4 and 55%, respectively.

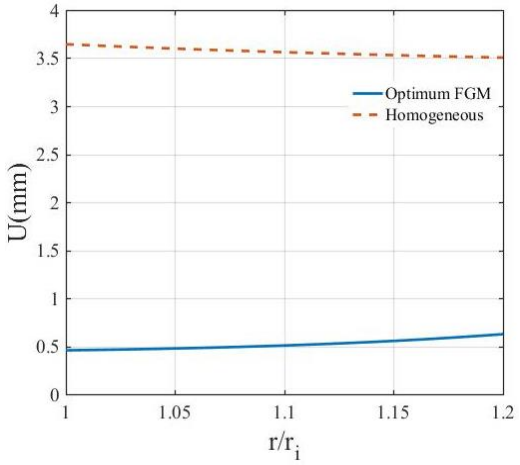

Fig. 9. Distribution of radial displacement in homogeneous and optimal FGM states

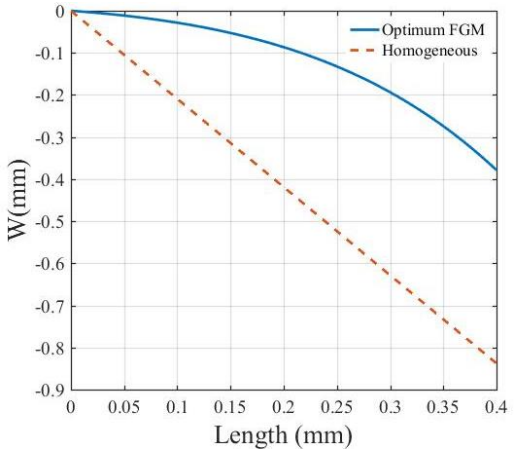

Fig. 10. Distribution of axial displacement in homogeneous and optimal FGM states

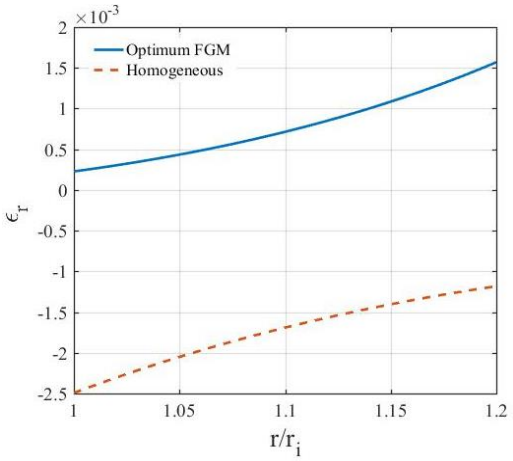

Fig. 11. Distribution of radial strains in homogeneous and optimal FGM states

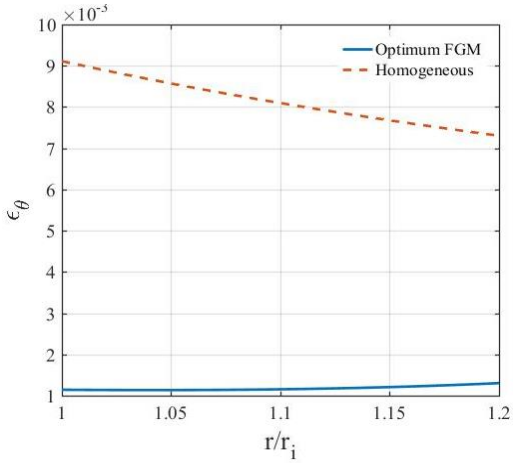

Fig. 12. Distribution of circumferential strains in homogeneous and optimal FGM states

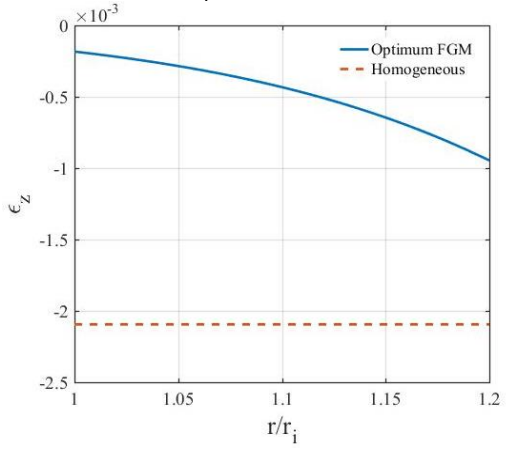

Fig. 13. Distribution of axial strains in homogeneous and optimal FGM states

Fig. 14 presents the distribution of temperatures of the spool in homogeneous and optimum FGM states along radius. In Fig. 15, the effect of the spool rotation speed variations on optimal coefficient (m) and equivalent safety factor have been investigated. Analysis was performed for different rotation

speeds under the same working conditions. It is known that in the case which the spool has no rotation speed, the optimal coefficient is -3 and, in this case, the safety factor is 22.8. By increasing rotational speed, the optimal coefficient decreases but does not exit from range of -10. In addition, by increasing the speed at each case, the value of safety factor in optimal state also reduced. Therefore, increasing the speed leads to a reduction in the safety factor.

In Fig. 16, the effect of changes in the type and number of blades and subsequently the equivalent external radial load on an optimal coefficient and equivalent safety factor has been investigated. Analysis is performed for different radial loads under the same working conditions. It is known that similar to the case of increasing the speed case, increasing the external radial load (blades equivalent load) will result in a reduction in safety factor. However, the optimal coefficient is still negative and is in the range of -10 to 0. However, it did not have any particular behavior. For example, by increasing load from 0 to 50 MPa, optimal coefficient reduced but from 50 MPa to 100 MPa, it increased.

In Fig. 17, the effect of changes in internal radial load on an optimal coefficient and equivalent safety factor has been investigated. Analysis is performed for different radial loads under the same working conditions. Increasing the internal radial load will result in a reduction in safety factor. How-ever, the optimal coefficient is still negative and is in the range of -10 to 0 and again, it did not have any particular behavior.

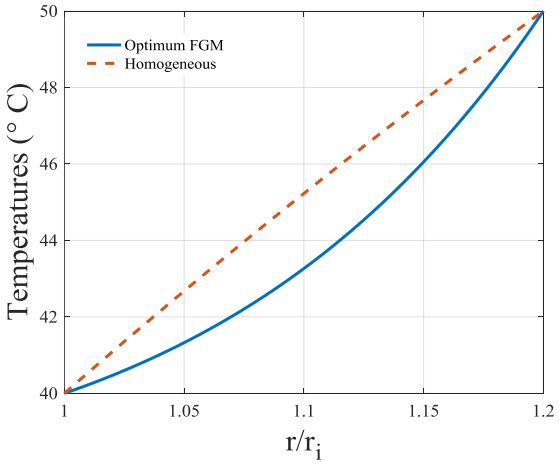

Fig. 14. Distribution of Von Mises equivalent stress in homogeneous and optimal FGM states

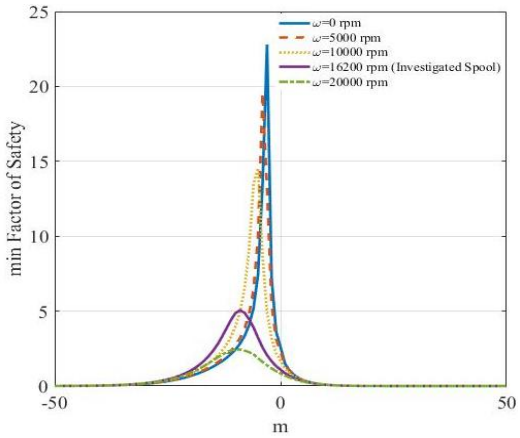

Fig. 15. Change in the spool safety factor by changing the FGM coefficient at different speeds

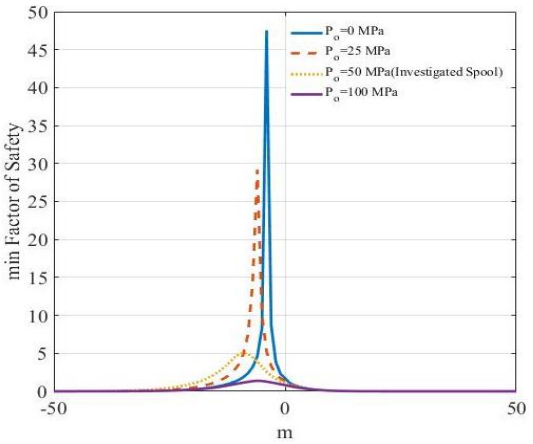

Fig. 16. Change in the spool safety factor by changing the FGM coefficient at different external loadings

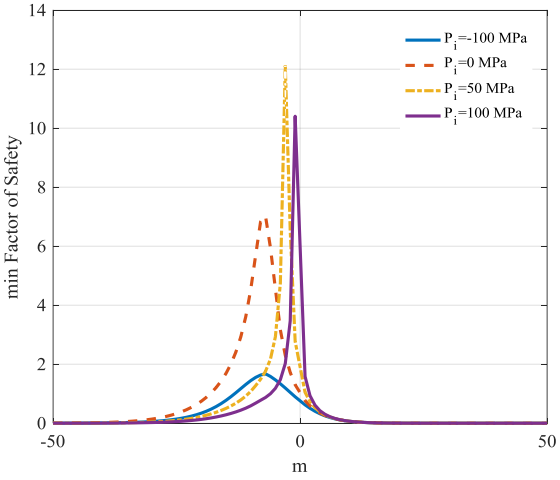

Fig. 17. Change in the spool safety factor by changing the FGM coefficient at different internal loadings

In Fig. 18, the effect of changes thickness on an optimal coefficient and equivalent safety factor has been studied. It can be seen that using more thick spools would lead to optimal states with fewer values of safety factor.

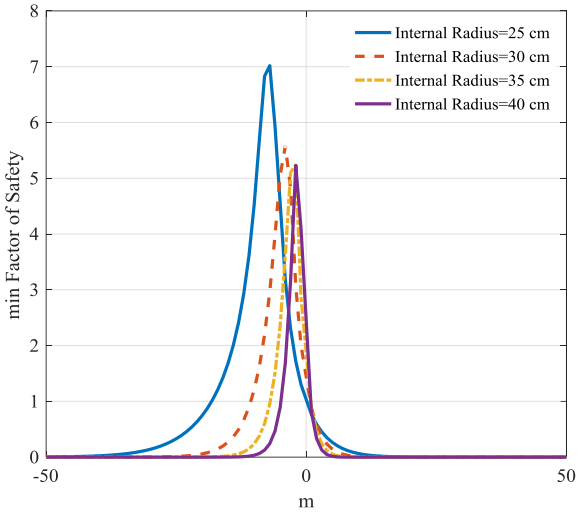

Fig. 18. Change in the spool safety factor by changing the FGM coefficient at different thicknesses

6. Conclusion

In this article, an exact analysis of the spool stresses, displacements, and strains in specified axial compressor has been investigated. The spool was analyzed under thermo-elastic loads and arbitrary thermal function. To consider a specific thermal function applying on the spool, heat conduction equation was solved and replaced. Obviously, the above analysis could be used in other thermal functions. In FGM state, the numerical optimization method was used to calculate the coefficient that gave the highest safety factor and the distribution of stresses, displacements, and strains under specific loading conditions in both homogeneous and optimal states has been investigated. The results indicated an improvement of 477% for a safety factor for FGM state in comparison with homogeneous state. Also, the maximum values of radial and axial displacements for FGM state in comparison with homogeneous state decreased by 87.44% and 54.6%, respectively. In addition, 89.68% reduction was observed for obtained optimal equivalent stresses results in comparison with homogeneous state. In radial, circumferential and axial strains, the maximum values of strains for optimal state have decreased by 37.35, 44.4 and 55%, respectively. The results show that the optimal coefficient changes with changing radial loading and rotation speed. For the considered spool particular geometry, optimal coefficient was -8.975. Also, it was found that increasing the radial external loading and the spool rotation speed leads to decrease in the safety factor or increase in equivalent stresses. In the analyzed coefficient range, the effect of increasing the blades loading on reducing equivalent safety factor is higher than rotation speed. The results indicate that increasing the internal loading values causes tending the optimal coefficient from negative values to zero, but using tensile loading instead of compression, would cause decrease in rate of optimal coefficient variations. Furthermore, increasing the thickness would cause tending the optimal coefficient from negative values to zero, and the higher thicknesses, have fewer values of safety factor due to their more centrifugal loadings.

Nomenclature

σ_r	Radial Stress
σ_θ	Circumferential Stress
σ_z	Axial Stress
ε_r	Radial Strain
ε_θ	Circumferential Strain
ε_z	Axial Strain
u	Radial Displacement
w	Axial Displacement
ω	Angular Velocity
N	Poisson's Ratio
E	Modulus of elasticity
ρ	Density
α	Thermal Expansion Coefficient
k	Thermal Conductivity
σ_y	Yield Strength
m	Non-Homogeneous Coefficient
r_i	Inner Radius of Spool
r_o	Outer Radius of Spool
$B_1 \sim B_7$	Stress parameters
P_i	Uniform Internal Loads
P_o	Uniform External Loads
$C_1 \& C_2$	Integral Constants
σ_{eq}	Von Mises Equivalent Stress
$A_1 \sim A_3$	Parameters of Motion Equation Solution
$D_1 \sim D_9$	Parameters of Integral Constants
T_i	Inner Surface Temperature
T_o	Outer Surface Temperature
h_i	Inner Heat Transfer Coefficient
h_o	Outer Heat Transfer Coefficient
β	Dimensionless Radial Coordinate
$T(r)$	Thermal Equation

References

[1] Nadai A. **Theory of Flow and Fracture of Solids**. 2nd ed. 1950.

[2] Timoshenko S, Goodier J. **Theory of Elasticity**. 3rd ed. New York: McGraw-Hill; 1970.

[3] Lamé G. **Leçons Sur La Théorie Mathématique De L'elasticité Des Corps Solides Par G. Lamé.** Gauthier-Villars; 1866.

[4] Fukui Y, Yamanaka N. Elastic Analysis for Thick-Walled Tubes of Functionally Graded

Material Subjected to Internal Pressure. *JSME international journal. Ser. 1, Solid mechanics strength of materials* 1992; 35(4): 379-385.

[5] Tutuncu N, Ozturk M. Exact solutions for stresses in functionally graded pressure vessels. *Composites Part B: Engineering* 2001; 32(8): 683-686.

[6] Rooney F, Ferrari M. Tension, Bending, and Flexure of Functionally Graded Cylinders. *International Journal of Solids and Structures* 2001; 38(3): 413-421.

[7] Galic D, Horgan C. The stress response of radially polarized rotating piezoelectric cylinders. *Transactions-American Society of Mechanical Engineers Journal of Applied Mechanics* 2003; 70(3): 426-435.

[8] Tutuncu N. Stresses in thick-walled FGM cylinders with exponentially-varying properties, *Engineering Structures*. 2007; 29(9): 2032-2035.

[9] Khoshgoftar M, Rahimi G, Arefi M. Exact Solution of Functionally Graded Thick Cylinder with Finite Length under Longitudinally Non-Uniform Pressure. *Mechanics Research Communications* 2013; 51: 61-66.

[10] Zamani Nejad M, Jabbari M, Ghannad M. A Semi-Analytical Solution for Elastic Analysis of Rotating Thick Cylindrical Shells with Variable Thickness Using Disk Form Multilayers. *The Scientific World Journal* 2014; 2014.

[11] Ghajar R, Shokrieh M, Shajari AR. Transient Thermo-Visco-Elastic Response of a Functionally Graded Non-Axisymmetric Cylinder. *Journal of Computational Applied Mechanics* 2015; 46(2): 191-204.

[12] Nejad MZ, Fatehi P. Exact Elasto-Plastic Analysis of Rotating Thick-Walled Cylindrical Pressure Vessels Made of Functionally Graded Materials. *International Journal of Engineering Science* 2015; 86: 26-43.

[13] Arefi, M, Nahas I., Abedi M. Thermo-Elastic Analysis of a Rotating Hollow Cylinder Made of Arbitrary Functionally Graded Materials. *Journal of Theoretical and Applied Mechanics* 2015; 45(4): 41-60.

[14] Jabbari M, Ghannad M, Nejad MZ. Effect of Thickness Profile and FG Function on Rotating Disks Under Thermal and Mechanical Loading. *Journal of Mechanics* 2016; 32(1): 35-46.

[15] Anani Y, Rahimi GH. Stress Analysis of Rotating Cylindrical Shell Composed of Functionally Graded Incompressible Hyperelastic Materials. *International Journal of Mechanical Sciences* 2016; 108: 122-128.

[16] Afshin A, Zamani Nejad M, Dastani K. Transient Thermoelastic Analysis of Fgm Rotating Thick Cylindrical Pressure Vessels under Arbitrary Boundary and Initial Conditions. *Journal of Computational Applied Mechanics* 2017; 48(1): 15-26.

[17] Gharibi M, Nejad MZ, Hadi A, Elastic Analysis of Functionally Graded Rotating Thick Cylindrical Pressure Vessels with Exponentially-Varying Properties Using Power Series Method of Frobenius. *Journal of Computational Applied Mechanics* 2017; 48(1): 89-98.

[18] Jalali M. H., B. Shahriari, Elastic Stress Analysis of Rotating Functionally Graded Annular Disk of Variable Thickness Using Finite Difference Method. *Mathematical Problems in Engineering* 2018;https://doi.org/10.1155/2018/1871674.

[19] Khorsand M, Tang Y. Design Functionally Graded Rotating Disks under Thermoelastic Loads: Weight Optimization. *International Journal of Pressure Vessels and Piping* 2018; 161: 33-40.

[20] Hosseini M, Dini A, Eftekhari M. Strain gradient effects on the thermoelastic analysis of a functionally graded micro-rotating cylinder using generalized differential quadrature method. *Acta Mechanica* 2017; 228(5): 1563-1580.

[21] Nkene, Elise Rose Atangana. Displacements, Strains, and Stresses Investigations in an Inhomogeneous Rotating Hollow Cylinder Made of Functionally Graded Materials under an Axisymmetric Radial Loading. *World Journal of Mechanics* 2018; 8(3): 59.

[22] Yaghoobi P, Ghaffari M, Ghannad G. Stress and active control analysis of functionally graded piezoelectric material cylinder and disk under electro-thermo-mechanical loading. *Journal of Intelligent Material Systems and Structures* 2018; 29(5): 924-937.

[23] Mehditabar A, Rahimi G.H., Tarahhomi M. H. Thermo-elastic analysis of a functionally graded piezoelectric rotating hollow cylindrical shell subjected to dynamic loads. *Mechanics of Advanced Materials and Structures* 2018; 25(12): 1068-1079.

[24] Hussain, Imad A, Lafta H, Rafa'a D. Thermo Elasto-Plastic Analysis of Rotating Axisymmetrical Bodies Using Modified Von-Mises Yield Criterion. *Al-Khwarizmi Engineering Journal* 2018; 4(4): 71-81.

[25] Vullo V, Vivio F. **Rotors: Stress Analysis and Design**. Springer Science & Business Media; 2013.

[26] Nejad MZ, Rahimi G. Deformations and Stresses in Rotating Fgm Pressurized Thick Hollow Cyl-

inder under Thermal Load. *Scientific Research and Essays* 2009; 4(3): 131-140.

[27] Nejad MZ, Jabbari M, Ghannad M. Elastic Analysis of Fgm Rotating Thick Truncated Conical Shells with Axially-Varying Properties under Non-Uniform Pressure Loading. *Composite Structures* 2015; 122: 561-569.

[28] Nejad MZ, Jabbari M, Ghannad M. Elastic Analysis of Axially Functionally Graded Rotating Thick Cylinder with Variable Thickness under Non-Uniform Arbitrarily Pressure Loading. *International Journal of Engineering Science* 2015; 89: 86-99.